Published in final edited form as:
IEEE Nucl Sci Symp Conf Rec (1997). 2011 ; : 4735–4738.

Multi-Material Decomposition using Low-Current X-Ray and a Photon-Counting CZT Detector

Sangtaek Kim,
Physics Research Laboratory, University of California, San Francisco, San Francisco, CA 94107 USA

Andrew Hernandez,
Physics Research Laboratory, University of California, San Francisco, San Francisco, CA 94107 USA

Fares Alhassen,
Physics Research Laboratory, University of California, San Francisco, San Francisco, CA 94107 USA

Michael Pivovaroff,
Lawrence Livermore National Laboratory, Livermore, CA 94550 USA

Hyo-Min Cho,
Yonsei University, Won-ju, South Korea

Robert G. Gould, and
Physics Research Laboratory, University of California, San Francisco, San Francisco, CA 94107 USA

Youngho Seo [Senior Member, IEEE]
Physics Research Laboratory, University of California, San Francisco, San Francisco, CA 94107 USA

Sangtaek Kim: sangtaek_kim@yahoo.com

Abstract

We developed and evaluated an x-ray photon-counting imaging system using an energy-resolving cadmium zinc telluride (CZT) detector coupled with application specific integrated circuit (ASIC) readouts. This x-ray imaging system can be used to identify different materials inside the object. The CZT detector has a large active area (5×5 array of 25 CZT modules, each with 16×16 pixels, cover a total area of 200 mm × 200 mm), high stopping efficiency for x-ray photons (~ 100 % at 60 keV and 5 mm thickness). We explored the performance of this system by applying different energy windows around the absorption edges of target materials, silver and indium, in order to distinguish one material from another. The photon-counting CZT-based x-ray imaging system was able to distinguish between the materials, demonstrating its capability as a radiation-spectroscopic decomposition system.

I. Introduction

Most of the current x-ray detectors using scintillators are coupled to charge collection devices (e.g., charge-coupled-device (CCD) or complementary–metal-oxide-semiconductor (CMOS)). These detectors measure the intensity of a transmitted x-ray beam by analog integration of the electrical signal from a radiation detector, where the integration includes the detector leakage current and charges induced by x-ray photons, obscuring the attenuation profile information from the x-ray.

The limitation of this type of detector is that it cannot evaluate the energy of individual incident photons or the attenuation properties of the transmitted object. In contrast, photon-counting solid-state detectors, such as cadmium zinc telluride (CZT) or cadmium telluride (CdTe), can both count and resolve the energy of the individual photons and thus they can provide the attenuation profile vs. energy of an imaged object [1]. These photon-counting solid-state detectors generally have both short charge collection times and good energy resolution. For x-ray imaging, they require fast-counting multi-channel parallel readout electronics, e.g., high-speed application-specific integrated circuits (ASICs) [2].

The high energy discrimination capability of a photon-counting detector can be used to differentiate the attenuation characteristics of various materials using a single polychromatic x-ray exposure and multiple energy windows [3],[4]. This might be a simpler and more efficient method to differentiate materials compared with using a dual-energy x-ray source[5]–[9]. The x-ray attenuation is a function of the incident photon energy and its nonlinear absorption profiles, which are unique for each material. The energy windowing of photon-counting detectors provides energy-selective x-ray projection images from a single x-ray exposure. In addition, different materials can be separated by applying multiple energy windows around nonlinear absorption edges (e.g. Kedge) [9]–[11].

In this study, we used a CZT detector developed originally as a gamma camera that was reconfigured for photon-counting and energy-resolved x-ray imaging. Using this imaging system, we evaluated the capability of decomposing different materials in x-ray projection images using multiple energy windows (above and below the K-edge energy) for each material, in particular discriminating silver and indium from other materials.

II. System description

We used a microfocus x-ray tube from Oxford Instruments (Scotts Valley, CA), which has a voltage range from 4 to 60 kVp, 1 mA maximum current, a maximum power of 60 W, and a 120 μm focal spot, for all experiments. The x-ray tube has a fixed anode, simple air cooling, and operated at a constant potential. The x-ray tube was 84.3 cm away from the CZT detector as shown in Fig. 1(a).

The CZT detector and two multi-channel ASICs readout electronics were developed and assembled by Gamma Medica, Inc. (Northridge, CA). The signals from the CZT are read out by two multi-channel ASICs. The CZT detector has a 20 cm×20 cm active area, is composed of 5 × 5 detector modules. Each module consists of a 16×16 array of 2.5 mm square pixels (80 × 80 total elements), providing discrete spatial position information. The thickness of the CZT crystal is 5 mm. The temperature of the detector was stabilized at 20° C by circulating ethylene glycol through plastic tubing around the detector elements. The CZT crystals, ASICs, and supporting electronics were enclosed inside an aluminum box for mechanical protection and electromagnetic shielding. The signals from ASICs are transformed by analog-to-digital converters (ADC) and transferred to a computer for readout. The CZT detector has a linear count rate response with a maximum count rate of 15,000 counts per second (cps). Thus, it is desirable to operate CZT at low count rate to avoid a pulse pile-up induced by multi-hit photons onto the detector [12].

Fig. 1(a) shows the layout of the projection imaging system. Fig. 1(b) shows the photograph of the system placed on a vertically standing rotational gantry. A lead collimator limited the x-ray beam at the detector to a 62.5 mm diameter circular area. The test objects were placed just in front of the detector. The collimator combined with low current x-ray flux incident on the detector, significantly reduced scattered photons as well as the multi-hit photons.

III. Attenuation coefficient and K-edge

Fig. 2 shows the calculated relative mass attenuation of silver and indium. The data (mass attenuation coefficient (μ/ρ [cm^2/g]) were retrieved from the XCOM database at the National Institute of Standards and Technology (NIST, Boulder, CO) [13]. The relative linear attenuation of each material is given by

$$\frac{I}{I_o}=\exp(-\mu \cdot t), \quad (1)$$

where I is the transmitted photons flux, I_o is the incident photons flux, μ is the linear attenuation coefficient of each material, which can be derived by multiplying the mass attenuation coefficient(μ/ρ [cm^2/g]) and the density of material(ρ [g/cm^3]), and t is the thickness (cm) of the material in the direction perpendicular to the detector plane. The K absorption edge of silver (25.5 keV) is lower than that of indium (27.9 keV). We can separate out these materials by applying an appropriate energy window for the projection image. At the energy window right above the K absorption edge, most of the photons from the x-ray tube will be absorbed by the material, generating high contrast between the background (transmitted photons) and the object (absorbed photons).

IV. Energy resolved image around the K-edge of the thin silver plate

We took a projection image of the thin silver plate (0.13 mm, 40 mm × 40 mm area) placed on the CZT detector surface. The x-ray tube was driven by a 45 kVp voltage and a 0.5 μA current. A lead collimator was placed on the detector, to decrease the count rate and thus the number of co-incident photons and thus, reduce the pulse-pile-up effect. The total counts for each projection image was ~9.4×10^6, requiring ~600 seconds of imaging, yielding a count rate of ~15,833 cps. A 60 mV threshold voltage was applied to CZT detector. The projection images were corrected for bad pixels and gain and offset variations among pixels.

After acquiring the projection image, we filtered the image with two different energy windows, one below the K-edge and one above the K-edge. Fig. 3(a) shows the projection image after applying a 21–24 keV energy window, which lies just below the K-edge of silver attenuation profile. There were a total ~2.4×10^6 collected photons. The dark area inside the circular collimator mask is due to absorption by the silver plate. A number of photons were detected inside the silver plate area due to x-ray photon penetration through silver plate. Fig. 3(b) shows the projection image of silver plate when the energy window was applied right above the K-edge (26–29 keV). The image has a well-distinguished shape of the square silver plate centered on the lead collimator. There were total ~1.8×10^6 of collected photons. To quantify the contrast between these two images, we summed up slices over 11 pixel rows and plotted the profile as shown in Fig. 6(a) and (b). The peak-to-valley ratio for the energy window below the K-edge shown in Fig. 6(c) is ~6, and the peak-to valley ratio for the energy window above the K-edge shown in Fig. 6(d)is ~23. From the slice profile, we can conclude that the 26–29 keV energy window has much better contrast-enhanced image of silver plate compared with the 21–24 keV energy window. The result indicates that a properly chosen energy window around the K-edge can significantly improve the contrast of the projection image.

V. Material decomposition demonstration by applying narrow energy window

We placed an indium plate (0.25 mm thickness, 15 mm × 40 mm area) next to a thick silver plate (0.25 mm thickness, 40 mm × 40 mm area) and took a projection image with a collimated x-ray beam (45 kVp, 0.0005 mA). After collecting photons for more than 10 minutes, we acquired the projection image and applied two different energy windows: one below and one above the K-edge of indium (27.9 keV). Fig. 4(a) shows the projection image with both indium and silver after energy filtering with a 24–26 keV window. More of the photons penetrated through the indium plate with the total number of collected photons was around ~9×10^5. The size and shape of the indium plate looks dim and unclear. On the other hand, when we applied the 28–30 keV energy window just above the K-edge of the indium, the indium plate stands out, generating a good contrast ratio from the background as illustrated in Fig. 4(b), where the total number of collected photons by the CZT detector was ~4.3×10^5. Fig. 4(c) and (d) show the profile of summed up slices (11 rows) of the projection image, where the summed region is indicated in Fig. 4(a) and (b). The profile of the below K-edge energy window shown in Fig. 4(c) has an elevated level of transmitted photons, thus having lower contrast from the background compared with the profile for the above-K-edge energy window shown in Fig. 4(d). The peak-to-valley ratio of the summed-up profiles at the below K-edge energy window shown in Fig. 4(c) is ~11, while that with the above-K-edge energy window shown in Fig. 7(d) is ~40. Thus, we can enhance the contrast of the indium plate by applying the energy window above the K-edge of the indium.

VI. Discussion

Enhancing the contrast of materials using proper energy windowing around the K-edge of target materials can be challenging due to the limited detector energy resolution. The energy resolution of photon-counting detectors is mainly affected by the noise properties of the detector, the pulse pile-up effect, and characteristic x-ray and spectral distortion caused by charge sharing between detector pixels. The energy resolution in the low energy range is worse than the higher energy range, and the narrow energy window used for filtering can cause artifacts and aliasing effects.

In this paper, the x-ray source specifications limited the applicable energy window to below 30 keV or so, which made us only focus on separating materials with K-edges around 20–30 keV. However, with a higher energy x-ray source, we could test materials with higher K-edges, such as gold (80.7 keV), which are currently being investigated in nanoparticle forms in medical imaging, or other materials of interest (explosive, hazardous) in for homeland security purposes. Gold is particularly of great interest, since it improves targeted therapeutic radiation delivery in the form of gold nanoparticles [14]–[16].

VII. Conclusion

We have built and tested a CZT-based photon-counting, energy-resolving x-ray detector for multi-material decomposition. We used polychromatic x-ray beam and utilized the spectral counting ability of the CZT detector to acquire the energy and spatial information of incident photons through different materials.

We have also shown that proper energy windowing around the K-edge of the material can substantially enhance the separation of some specific materials (e.g. silver and indium) even with the detector's finite energy resolution and the pulse pile-up and charge sharing effects. Our results imply that the differentiation of various materials is possible using this kind of

imaging setup, which can be applied to improved x-ray CT imaging or homeland security for hazardous material detection.

Acknowledgments

This work was supported in part by the National Institutes of Health under grant R01 EB000348 and grant R01 EB012965.

References

1. Takahashi T, Watanabe S. Recent Progress in CdTe and CdZnTe detectors. IEEE Trans Nucl Sci. 2001; 48(4):950–959.
2. Beuville E, Cederström B, Danielsson M, Luo L, Nygren D, Oltman E, Vestlund J. An application specific integrated circuit and data acquisition system for digital X-ray imaging. Nucl Instrum Methods Phys Res A. 1998; 406:337–342.
3. Wang X, Meier D, Mikkelsen S, Maehlum GE, Wagenaar DJ, Tsui BMW, Patt BE, Frey EC. MicroCT with energy-resolved photon-counting detectors. Phys Med Biol. 2011; 56:2791–2816. [PubMed: 21464527]
4. Wang X, Meier D, Taguchi K, Wagenaar DJ, Patt BE, Frey EC. Material separation in x-ray CT with energy resolved photon-counting detectors. Med Phys. 2011; 38:1534–1546. [PubMed: 21520865]
5. Lehmann LA, Alvarez RE, Macovski A, Brody WR, Pelc NJ, Riederer SJ, Hall AL. Generalized image combinations in dual kVp digital radiography. Med Phys. 1981; 8:659–667. [PubMed: 7290019]
6. Alvarez RE, Seibert JA, Thompson SK. Comparison of dual energy detector system performance. Med Phys. 2004; 31:556–565. [PubMed: 15070254]
7. Primak AN, Ramirez Giraldo JC, Liu X, Yu L, McCollough CH. Improved dueal-energy material discrimination for dual-source CT by means of additional spectral filtration. Med Phys. 2009; 36:1359–1369. [PubMed: 19472643]
8. Saito M. Spectral optimization for measuring electron density by the dual-energy computed tomography coupled with balanced filter method. Med Phys. 2009; 36:3631–3642. [PubMed: 19746797]
9. Feuerlein S, Roessl E, Proksa R, Martens G, Klass O, Jeltsch M, Rasche V, Brambs HJ, Hoffmann MHK, Schlomka JP. Multienergy Photon-counting K-edge Imaging. Radiology. 2008; 249:1010–1016. [PubMed: 18849505]
10. Roessl E, Proksa R. K-edge imaging in x-ray computed tomography using multi-bin photon counting detectors. Phys Med Biol. 2007; 52:4679–4696. [PubMed: 17634657]
11. Schlomka JP, Roessl E, Dorscheid R, Dill S, Martens G, Istel T, Bäumer C, Herrmann C, Steadman R, Zeitler G, Livne A, Proska R. Experimental feasibility of multi-energy photon-counting K-edge imaging in pre-clinical computed tomography. Phys Med Biol. 2008; 53:4031–4047. [PubMed: 18612175]
12. Sun, M. Phd dissertation. University of California; Berkeley: 2006. Development of a combined microSPECT/CT system for small animal imaging.
13. http://physics.nist.gov/PhysRefData/XrayMassCoef/tab3.html
14. Cormode DP, Skajaa T, van Schooneveld MM, Koole R, Jarzyna P, Lobatto ME, Calcagno C, Barazza A, Gordon RE, Zanzonico P, Fisher EA, Fayad ZA, Mulder WJM. Nanocrystal core high-density lipoproteins: A multimodality contrast agent platform. Nano Lett. 2008; 8:3715–3723. [PubMed: 18939808]
15. Cormode DP, Roessl E, Thran A, Skajaa T, Gordon RE, Schlomka JP, Fuster V, Fisher EA, Mulder WJM, Proksa R, Fayad ZA. Atherosclerotic plaque composition:analysis with multicolor CT and targeted gold nanoparticles. Radiology. 2008; 256(3):774–782. [PubMed: 20668118]
16. Popovtzer R, Agrawal A, Kotov NA, Popovtzer A, Balter J, Carey TE, Kopelman R. Targeted gold nanoparticles enable molecular CT imaging of cancer. Nano Lett. 2008; 8:4593–4596. [PubMed: 19367807]

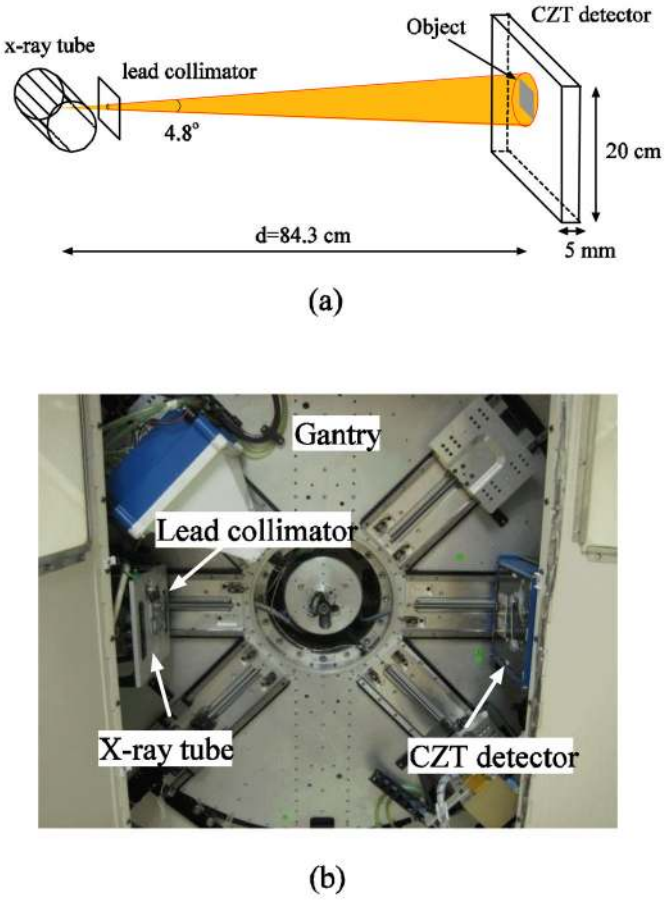

Fig. 1.

a) Schematic diagram of experimental setup. Conebeam(20° angle) x-ray source is placed 84.3 cm away from CZT detector. b) Photograph of the experimental setup with the x-ray tube on the left and CZT detector on the right, both mounted on a vertically-standing rotational gantry.

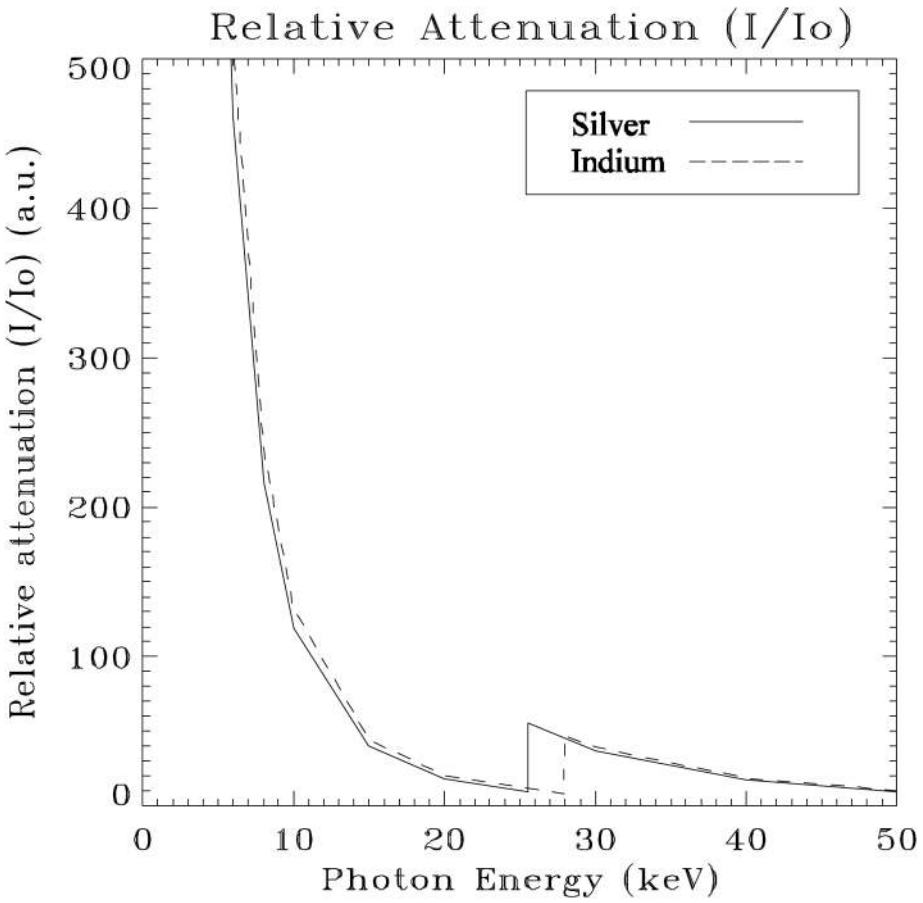

Fig. 2.
Attenuation profiles of silver (0.25 mm) and indium (0.25 mm). The K-edge of silver, and indium are at 25.5 and 27.9 keV.

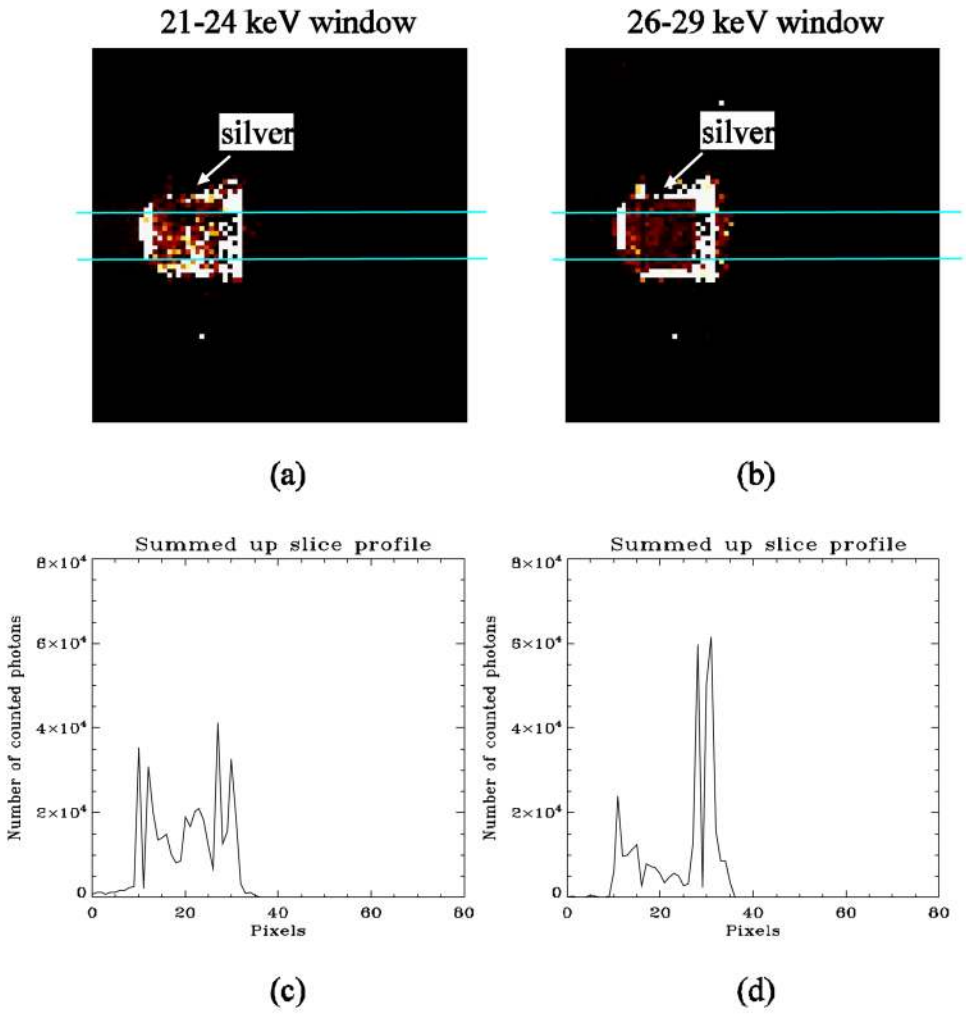

Fig. 3.

(a) Projection image of the thin silver plate with the 21–24 keV energy window. (b) Projection image of the silver plate with the 26–29 keV energy window. (c) Summed profile of the image of the silver plate projected through a collimator with 21–24 keV energy window. The location is indicated in (a). (d) Summed profile of the image of the silver plate projected through a collimator with a 26–29 keV energy window. The location is indicated in (b).

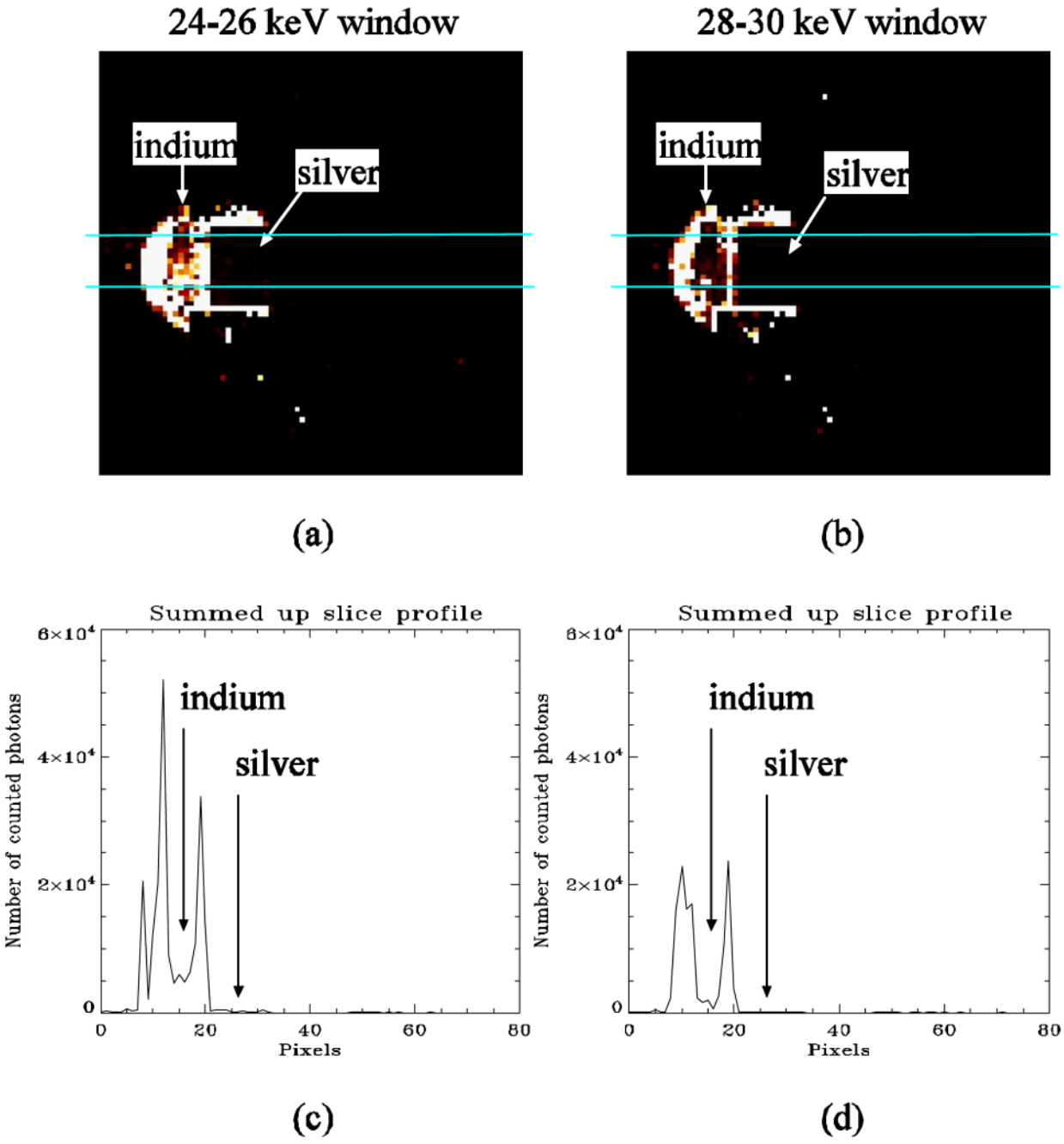

Fig. 4.

(a) Projection image of the silver and indium plates with the 25–28 keV energy window. (b) Projection image of the silver and indium plate with frequency range from 29–31 keV. (c) Summed profile of the image of the silver and indium plate projected through a collimator with the 24–26 keV energy window. The location is indicated in Fig. 4(a). (d) Summed profile of the image of the silver plate projected through a collimator with the 28–30 keV energy window. The location is indicated in (b).